$Cd_{0.7}Zn_{0.3}S$ NCs. These samples have been prepared successfully by using chemical co-precipitation method.

6.2 Experimental Details

6.2.1 Chemicals used

Cadmium acetate dihydrate ($Cd(CH_3COO)_2.2H_2O$), Triethylamine ($N(CH_2CH_3)_3$), copper-acetate monohydrate ($Cu(CH_3COO)_2.H_2O$), manganese-acetate tetrahydrate ($Mn(CH_3COO)_2.4H_2O$) and urea (NH_2CONH_2) have been purchased from the Sigma Aldrich. Zinc acetate dihydrate ($Zn\ (CH_3COO)_{2.}2H_2O$) and thiourea (NH_2CSNH_2) were consumed used as the for source material of Zn and S ions and these have been produced by the Loba Chemie.

6.2.2 Precursors preparations

Double distilled water has been used as a suitable solvent for all required chemical reactions. Acetate group was used as a precursor. Approximately 0.5 M cadmium-acetate and zinc-acetate have been taken according to their molar ratio in a clean beaker and added 100 ml double distilled water and stirred about half an hour at a fix temperature 60°C. In an second beaker or conical flask (500ml) 1M urea, 1M thiourea were taken and then dissolved in 100 ml of double distilled water and stirred it for half an hour under normal stirring rate 450 rpm.

6.2.3 Synthesis process

In order to prepare undoped $Cd_{0.7}Zn_{0.3}S$ we took x=0.3 i.e there was 30% of zinc and 70% of cadmium. Further in the conical flask solution 8 ml triethylamine has been added during vigorous fix stirring condition up to half an hour at 60°C for. After 10 minute stirring, precursor's solution of first beaker has been taken in a burette and mixed drop-wise into second beaker under vigorous stirring at 60°C. The drop rate were kept minimum (20 drops per minute) so that the drop completely mix in the solutions under stirring rate 990 rpm (revolution per minute). Consequently, solution changes from light yellow color to deep yellow during the reaction. As stirring completed the precipitates has been left untouched and undisturbed for one day and then were washed and filtered. After that the precipitates were dried in air oven at 90°C for 8 hours, to remove water, organic capping agent and other byproducts produced during the reaction. In the last, they were crushed in powder form using with the help of

a pestle-mortar and then utilized for various characterization. By following the same procedure, all the samples were prepared by taking dopant and co-dopant at different temperature. These powders were air annealed at 150°C, 250°C, 350° C for 2 h with a ramp rate 5°C/min and collected in airtight containers and then used for all measurements. By adopting the same procedure, five different samples were synthesized and coded their names as T1, T2, T3, T4 and T5 with respect to the material composition $Cd_{0.7}Zn_{0.3}S$; $Cd_{0.7}Zn_{0.3}S$ (350°C); $Cd_{0.7}Zn_{0.3}S$:Cu(250°C); $Cd_{0.7}Zn_{0.3}S$:Cu(350°C) and $Cd_{0.7}Zn_{0.3}S$:Cu,Mn(350°C) respectively. This nomenclature of our samples was used same throughout the chapter to avoid complexity. The complete annealing process has been shown in Fig 6.1 by a flow chart given below.

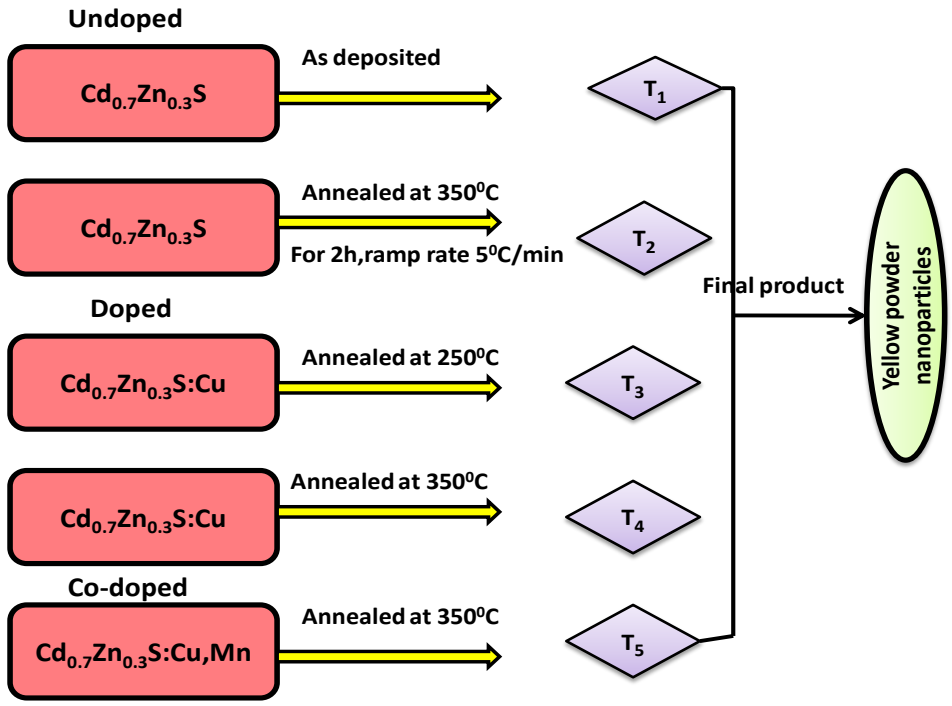

Fig. 6.1: Flow chart for synthesis at different annealing temperature of different samples.

6.2.4 Characterization

The XRD patterns of our powder form samples have been measured on a XRD X'Pert PRO with CuKα (λ=0.15406 nm) radiation at an operating voltage 45 kV and operating current at 40 mA with a scanning rate 2 degree min^{-1} from 2θ =20º to 60º. Further, a SHIMADZU IR Affinity-1 FTIR-spectrometer was used in the range 400-4000 cm^{-1} to identify of various functional groups present in the precursors. For FTIR investigations, the samples were mixed homogeneously with KBr (nine parts of KBr and one part of powder sample) and pellets of the desired dimensions were prepared under a pressure

of about 7 ton. Furthermore, morphological point of view of synthesized samples was also observed on a FEI TECNAI G^2 high resolution transmission electron microscope (HRTEM) operated at 200 kV. However different samples were prepared for TEM observations by dispersing in ethanol and then kept in a sonicator up to five minutes. After that the solution was dripped onto a carbon coated copper grid and dried at room temperature. Moreover, the optical absorption spectra of our prepared samples have been measured with the help of UV-VIS-NIR Spectrophotometer (Varian Cary-5000) in wide range 200-800 nm. For recording of absorption spectra, these samples have been prepared by dissolving 0.011 gm powder of the synthesized materials in 5 ml of ethanol. This was done by putting solution up to 5 minutes in the ultrasonic machine so that samples dispersed well and then used for UV-Visible measurements. In order to find the photoluminescence emission spectra Varian/ Perkin Elmer, Model: CARY-Eclipse/ LS-50B have been used. However, the excitation wavelength was selected from the absorption peak wavelength of UV-visible spectra for each prepared sample and thus their emission spectrums were measured in the range between 400-700 nm.

6.3 Results and Discussion

6.3.1 XRD analysis

The XRD analysis gives the information for structural properties by measurements of peak intensity, peak position, and FWHM and lattice plane. Structural type parameters as lattice parameters, particle size, dislocation density, and lattice structure, unit cell volume, lattice strain, and crystalline nature of the materials have been determined. Fig 6.2 exhibits the XRD pattern of as prepared, Cu doped and Cu,Mn doped $Cd_{0.7}Zn_{0.3}S$ samples at 350°C. The sample T4 have diffraction peaks at 2θ~ 25.31º, 26.94º, 28.33º, 44.42º, 48.56º and 52.68º corresponding to the (100), (002), (101), (110), (103) and (200) orientation or hkl planes respectively. The value of 2θ for sample T1, T2, T3, T4 and T5 corresponding to the (002) plane was given in the table 6.1. The diffraction peaks are found well matched by comparing with JCPDS card no. 40-0835 and 40-0836. The peaks of XRD of all samples have been found to good polycrystalline type nature of our prepared nanomaterials. The orientation in (002) hkl plane is the preferred direction in all the samples. Further, broadening of the XRD peaks indicates the formation of CdZnS nanocrystallites (NC's). The nanocrystals exhibited smaller number of lattice planes as comparison to bulk form that contributes to the broadening

of peaks in the diffraction pattern. This broadening in the XRD peaks may be due to the different type of crystal defects like dislocation and twinning [11]. The broadening in Cu-doped samples decreases in comparison to undoped, but in Cu,Mn doped (T5) sample at 350°C again broadening has increased and crystallite size decreases. This may be interpreted on the basis of ionic radii size of Mn^{2+} ion (0.67 Å) is less than the Cd^{2+} (0.97 Å) ion [12]. However, intensity of diffraction peak for sample T5 of all the planes has decreased due to the presence of Cu,Mn ions and it has also been observed that the plane (100) and (101) were intermixed and only (002) plane becomes orientation plane. Crystal structure of all our samples were found to be wurtzite or in hexagonal form. The lattice parameter, interatomic spacing, c/a ratio, volume of unit cell, particle size, strain, dislocation density have also been determined by using the XRD peak as given in the table 6.1 and 6.2. However, the crystallite size has been calculated by use of Debye Scherrer equation.

$$D=K\lambda/\beta Cos\theta \qquad (6.1)$$

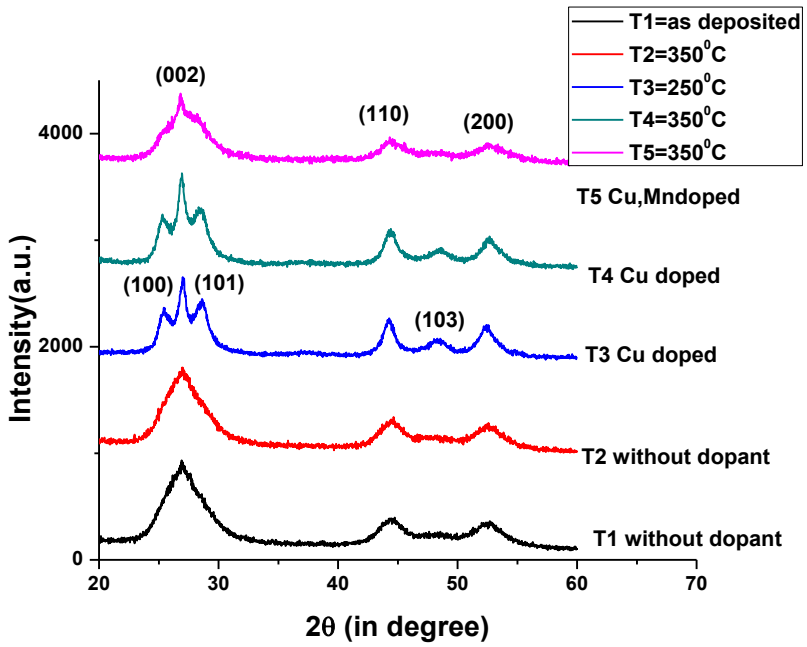

Fig. 6.2: XRD pattern of $Cd_{0.7}Zn_{0.3}S$ at different dopant and temperature.

The value of lattice constants 'a' and 'c' for hexagonal phase [13] of all the alloy samples have calculated to use the equation (6.2) and its value were mentioned in the table 6.1.

$$1/d^2 = 4/3(h^2+hk+k^2)/a^2+l^2/c^2 \qquad (6.2)$$

The values of lattice parameter are further refined by using the check cell program. The refined value of 'a' and 'c' and 2θ for sample T1, T2, T3, T4 and T5 are given in table 6.1. It has been observed that the calculated values of lattice parameter are almost same to the refined value. The changes in difference are very small. The unit cell volume [14] for hexagonal structure has been determined using equation (6.3) and value of Lorentz factor for our samples under this work was also calculated from the relation (6.4) as given below:

$$\mathbf{V = \sqrt{3}/2.a^2c} \qquad \mathbf{(6.3)}$$

$$\mathbf{L = 1/4\sin^2\theta\cos\theta} \qquad \mathbf{(6.4)}$$

Table 6.1: Structural parameters of the prepared samples.

Sr. No.	**Sample description**	**Peak Position (2θ)**		**a(Å)**		**c(Å)**		**c/a**	**d (Å)**	**Volume of unit cell (Å)^3**
		Obs.	Ref.	Obs.	Ref.	Obs.	Ref.			
T1as deposited	$Cd_{0.7}Zn_{0.3}S$	26.91	26.89	4.067	4.070	6.618	6.622	1.627	3.309	94.84
T2(350ºC)	$Cd_{0.7}Zn_{0.3}S$	26.96	26.95	4.053	4.055	6.605	6.607	1.629	3.303	94.01
T3(250ºC)	$Cd_{0.7}Zn_{0.3}S$:Cu	26.99	26.98	4.086	4.086	6.603	6.597	1.616	3.301	95.51
T4(350ºC)	$Cd_{0.7}Zn_{0.3}S$:Cu	26.94	26.89	4.073	4.073	6.611	6.621	1.623	3.305	95.05
T5(350ºC)	$Cd_{0.7}Zn_{0.3}S$:Cu,Mn	26.88	26.79	4.083	4.082	6.645	6.646	1.627	3.322	95.96

The lattice strain present in the nanocrystallites is determined from the XRD intensity peaks by using formula [15]

$$\boldsymbol{\varepsilon = \beta_{hkl}/4\,Tan\theta} \qquad \mathbf{(6.5)}$$

It was observed that in sample T1 without dopant and as deposited, the value of lattice strain and dislocation density have been found high (**ε** =0.0648, δ= 0.07980) in comparison to the doped and annealed samples as given in the table 6.2. The least strain has been obtained in the case of only Cu doped sample (T3); $Cd_{0.7}Zn_{0.3}S$ at 250°C as compared to the undoped T1, T2 (350°C) and co-doped T5(350°C) samples. However in the case of codoped samples T5(350°C); $Cd_{0.7}Zn_{0.3}S$:Cu(0.01M),Mn(0.01M) comparatively less strain found than undoped samples T1 as deposited and T2 (350°C), given in the table 6.2.

Table 6.2: Nanocrystallite size, microstrain and dislocation density and Lorentz factor of samples.

Sample	Crystallite size (nm)	Strain ε	Dislocation density $1/<D>^2$ (cm^{-2})	Lorentz Factor (L)
T1as deposited	3.54	0.0648	0.0798	4.748
T2(350°C)	4.17	0.0566	0.0575	4.732
T3(250°C)	9.01	0.0138	0.0123	4.728
T4(350°C)	11.76	0.0242	0.0072	4.739
T5(350°C)	4.21	0.0529	0.0564	4.786

Hence it have been concluded that the lattice strain and dislocation density decreases with temperature. This has also to be explained that with temperature surface defects are reduced [16]. The same type of experimental results were also found by A.Bakhsh et al. in which CdZnS thin films at 300°C and 400°C have decreased value of strain and dislocation density [6].

6.3.2 FTIR analysis

The FTIR spectra of undoped, Cu doping and Cu, Mn co doping samples were shown in the Fig 6.3. An absorption band is found at 3326-3410 cm^{-1} in higher energy region that corresponds to the O-H stretching vibration of water molecules on surface that appear for all the samples. However due to water evaporation this absorption is not sharp. The absorbance peak around 1634 cm^{-1} related to C-H stretching vibration [15]. However in lower energy region a small peak at wave number 657-676 cm^{-1} has been assigned to Cd-S/Zn-S stretching mode [17,18] and it becomes deeper for samples T3, T4 and T5. The absorption peak starts at 1390 cm^{-1} and has shifted to the 1421 cm^{-1} for the samples under investigations due to the symmetric stretching and 1564-1533 cm^{-1} presents the asymmetric stretching of the COO- of acetate group used in the precursor [19,20]. The absorption peak at 1533 cm^{-1} shifts slightly at higher wavelength and also becomes sharper for the samples T2, T4 and T5. The weak peak at wave number 2002-2032 cm^{-1} may be due to some microstructural deformation present in the samples. Peaks around 1135 cm^{-1} are appeared due to the characteristic frequency of inorganic ions and indicate the existence of resonance type interaction between vibrational modes of sulphide ions in the nanocrystal [21].

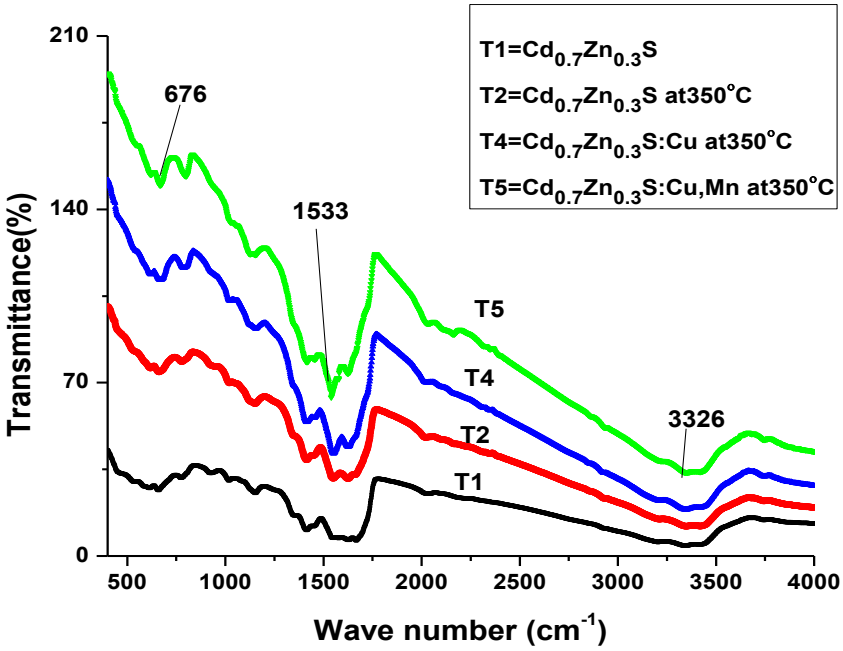

Fig. 6.3: FTIR spectra of $Cd_{0.7}Zn_{0.3}S$ without dopant, single dopant and codopant at 350°C temperature.

6.3.3 TEM analysis

Transmission electron microscopy (TEM) was employed to investigate for the morphology like size, shape, distribution and agglomeration of particles if present, of our prepared samples. The TEM images given in Fig. 6.4 show the spherical shape and nonhomogeneous distribution of nanoparticles. It was found that TEM with Cu doped and Cu,Mn codoped (Fig. 6.4) at 350°C shows agglomeration of particles. This agglomeration of particles in sample T5 is high because in this case the particle size is small as compared to single Cu doped at 350°C and surface energy of the particles increases that further increases agglomeration of the sample. In order to prevent agglomeration in the prepared samples some surfactant or capping agent must be used. These surfactants stabilize the particles by removing the dangling bond present at the surface of samples and also increase the luminescence efficiency or quantum yield.

The selective area electron diffraction (SAED) pattern of sample T4 has depicted in the inset which exhibits a set of rings rather than spots due to random orientation of crystallites, confirms polycrystalline nature of the material [22]. Effect of temperature on the TEM images has been clearly observed from the TEM micrograph given as in

the Fig 6.4 (b), (c), (d). Moreover, TEM histogram presents the graph between particle size and frequency of particles. By using these TEM images particle size have been calculated and its value for samples T1, T2, T4 and T5 are obtained 4.05, 5.0, 17.9 and 10 nm respectively. The size distribution by these histograms has been fitted with the Gaussian distributions. It has been observed that the particle size of sample T1 and T2 are found in close agreement with that determined by XRD method but for sample T4 and T5 particle size is larger than the XRD. This may be observed due to the fact that the TEM give the particle size not grain size while XRD give the crystallite or grain size. Particle is formed by number of grains [23], hence the particle size is larger than the grain size. The average value of crystallite size was found generally much smaller as compared to the other methods like TEM and UV [24]. Furthermore, grain size determined from XRD peak broadening is as a consequence of the contributions of the lattice defects, lattice strain and instrumental broadening.

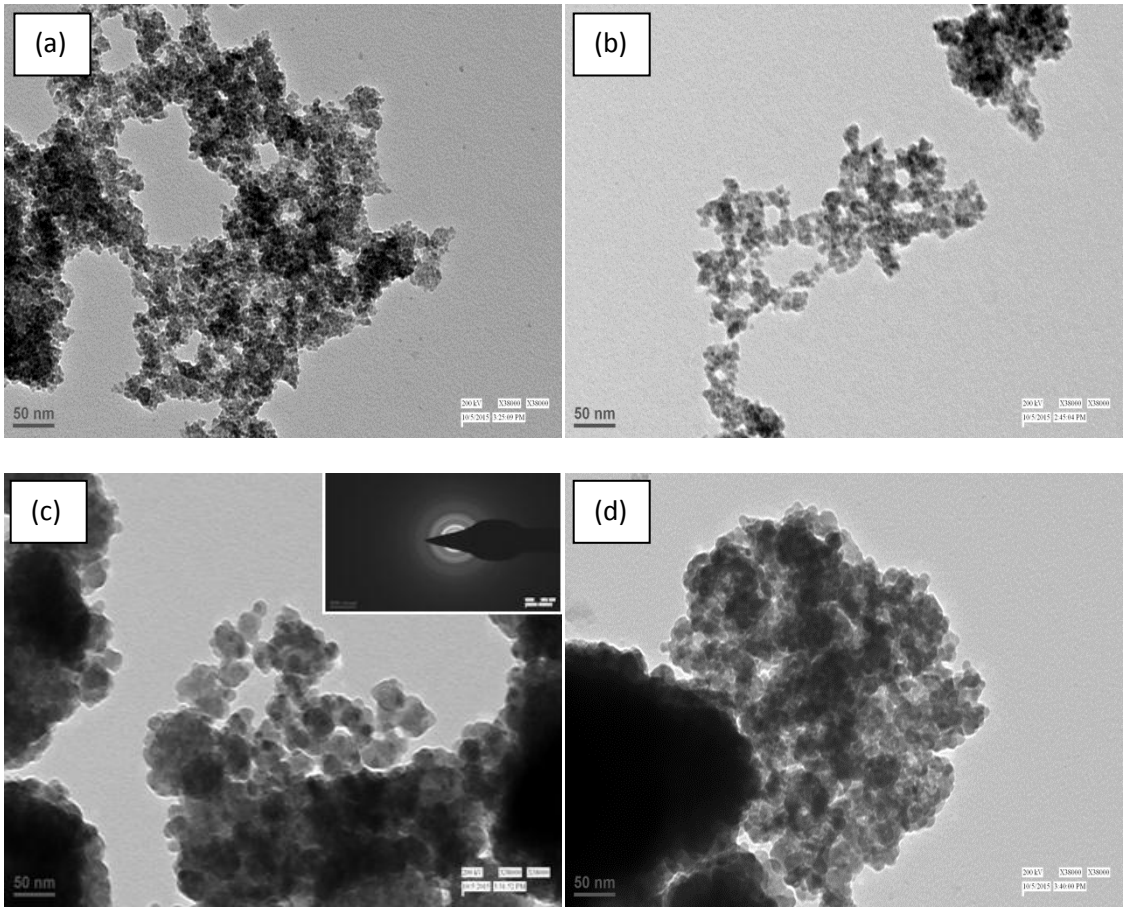

Fig. 6.4: TEM micrographs of undoped (a) $Cd_{0.7}Zn_{0.3}S$, (b) $Cd_{0.7}Zn_{0.3}S$ (350°C), single doped (c) $Cd_{0.7}Zn_{0.3}S$:Cu (350°C) and codoped (d) $Cd_{0.7}Zn_{0.3}S$: Cu, Mn (350°C) ternary alloy.

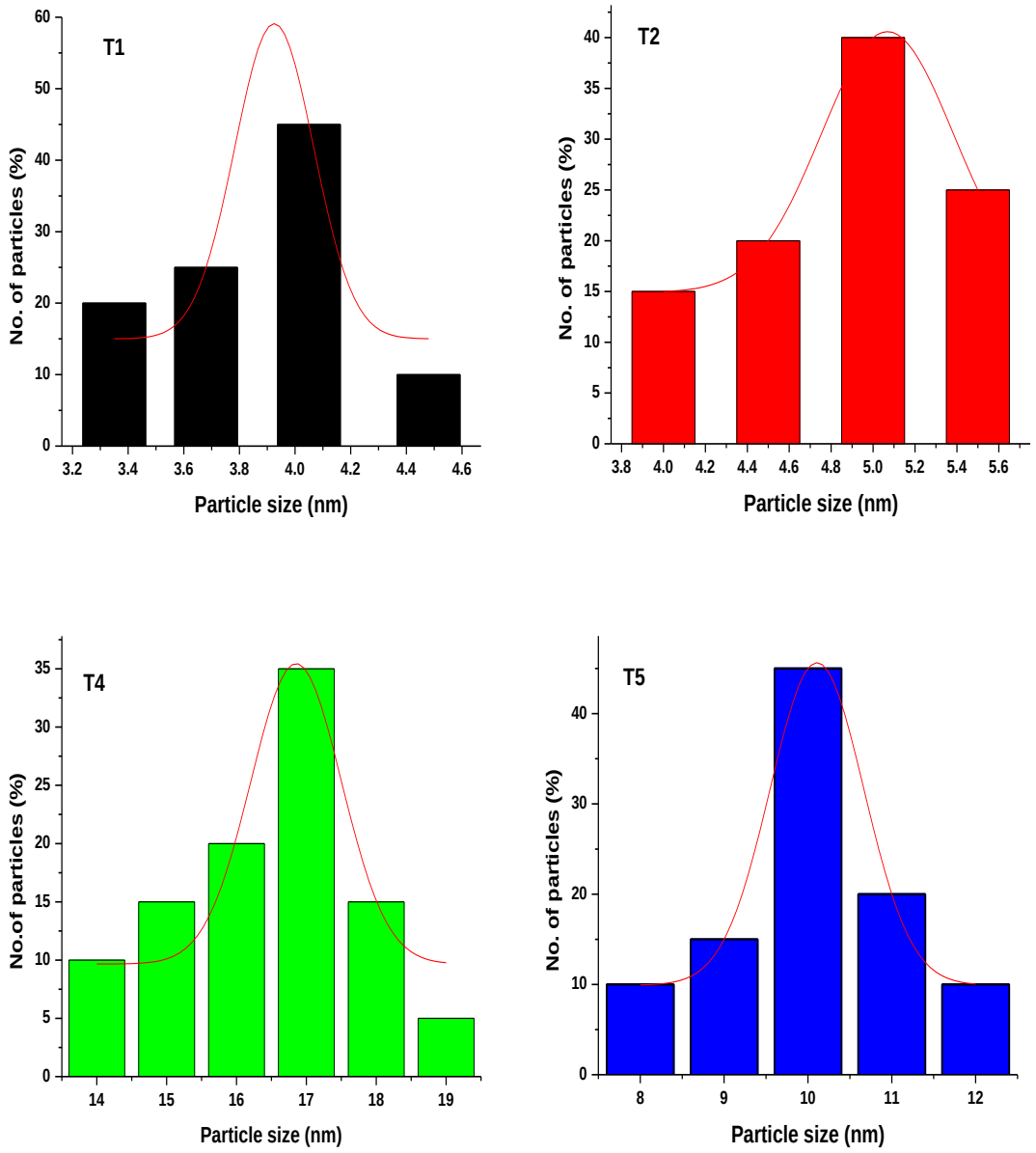

Fig. 6.5: Histograms of undoped (a) $Cd_{0.7}Zn_{0.3}S$, (b) $Cd_{0.7}Zn_{0.3}S$ (350°C), single doped (c) $Cd_{0.7}Zn_{0.3}S$:Cu (350°C) and codoped (d) $Cd_{0.7}Zn_{0.3}S$: Cu, Mn (350°C) ternary alloy.

6.3.4 UV-visible analysis

The spectra of optical absorption of our prepared samples were observed at room temperature in the range 200-800 nm as shown in the Fig.6.6 (a). The strongest absorption peak for the sample $Cd_{0.7}Zn_{0.3}S$ (T1) is observed at wavelength 245 nm which indicates the beginning of absorption and its absorption peak is found blue shifted as compared to bulk form of CdZnS, because basic absorption edge of bulk CdS

and ZnS has been reported at wavelength 513.6 nm and 340 nm respectively [25,26]. The appearance of blue shift may be interpreted on the basis of quantum size effect. From Fig 6.6 (a) absorption peak for sample T2, T4 and T5 were observed at the same wavelength 214 nm. However, the absorption edge of sample T1, T2, T4 and T5 lying at wavelength 259nm, 267nm, 261nm, 267nm respectively. A red shift was observed in the absorption edge as compared to the undoped sample T1, as a result of doping. Furthermore, no sharp absorption is observed, however small shoulder absorption appeared at 484 nm in sample T4 and T5 [27]. Moreover, the absorption is observed to decrease with the increase in wavelength for all our samples under investigations.

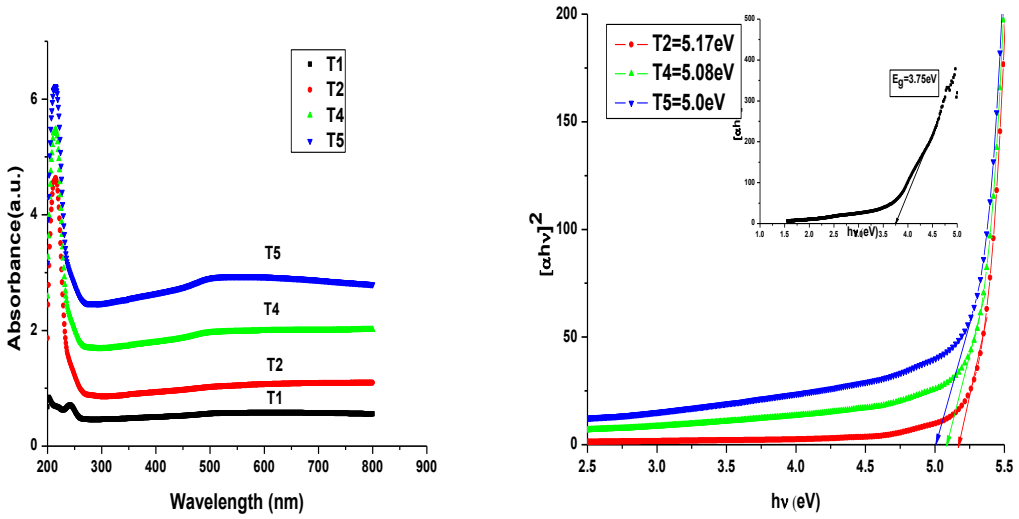

Fig. 6.6: (a) UV absorption spectra and (b) band gap energy of undoped (T1 as deposited) and doped (T2,T4,T5) of $Cd_{0.7}Zn_{0.3}S$ nanomaterials ternary alloy at 350°C.

Since the materials which we have prepared is a direct band gap type material, so the absorption coefficient for a direct band gap material near the band edge is calculated by the Tauc relation [28].

$$\alpha h\nu = A(h\nu - E_g)^n \qquad (6.6)$$

Here A is a constant and E_g is the band gap energy of the materials. Here n can have values 1/2 or 2 or 3/2 or 3 and we used n=1/2 for direct transition in our thesis work as described earlier in chapter 3. The energy band gap calculated from the Tauc relation by extension of linear portion of the plots to $(\alpha h\nu)^2 = 0$ have been depicted in the Fig 6.6 and their values for the sample T1 (shown in inset) T2, T4 and T5 are determined 3.75, 5.17, 5.08 and 5 eV, respectively. Energy band gap value for undoped samples is obtained smaller than the annealed and doped samples [29]. The same type result has

also been published by Kukreja et al., in that case 12.76% increment in the energy band gap of Mg-doped ZnO alloy at 14% Mg concentration was observed. However from the reported literature it has been observed that with doping band gap decreases [30,31] . On the other hand in our case with doping and annealing band gap increases (T1< T2,T4,T5) [32]. However except sample T1 the same trend is followed i.e T2 sample (annealed at 350°C) have higher band gap energy than T4 (Cu doped) and T5 (Cu, Mn doped). Further, material composition dependent band gap energy $E_{g,}$ of $Cd_{1-x}Zn_xS$ powder can be evaluated from the relation (6.7) for x=0.3 as reported by A.M. Salem [33].

$$\mathbf{E_g = 2.337 + 0.72x + 0.563x^2} \qquad \mathbf{(6.7)}$$

The value of band gap energy E_g calculated from above relation was reported to be 2.6 eV. This reported value of energy band is less than the above calculated samples from Tauc relation which also indicate that our prepared samples are nanomaterials because in nano the band gap increases due to quantum confinement effect.

6.3.5 Photoluminescence (PL) spectroscopy

Photoluminescence spectroscopy is a non-destructive optical technique used for measuring the band gap of materials, color of emission and detection of point defects. In photoluminescence process the sample were irradiated with photons of energy greater than the band gap energy $hv>E_g$ of that material. In the recombination process energy will transform partly into non-radiative transition (in the form of heat) and partly into radiative emission (emission of photons in visible range). The photon energies reflect the presence of different energy states that are found in the semiconductor. Various energy states produced in a crystal by a number of defects and also from impurities introduced in the lattice.

The PL spectra of $Cd_{0.7}Zn_{0.3}S$:Cu and $Cd_{0.7}Zn_{0.3}S$:Cu,Mn annealed at 350°C were shown in the Fig 6.7. The value of excitation wavelength of our samples was estimated from the UV-visible absorption spectra and by taking the same we observed the emission spectra. From the PL spectra (Fig 6.7) it has been observed that only Cu doped (T4) sample show two emission peak at 428 nm (blue emission) and 488 nm (green emission). These two emissions peaks are due to sulphur vacancies and zinc defects respectively presents in the system material [34,35]. Although, these two bands of emission in Cu doped ZnS were also observed by many researchers. Moreover, Changqing Jin et al. have reported that in $Zn_{0.7}Cd_{0.3}S$ nanobelts after annealing show

two emission peaks at 400 nm and 550 nm attributed to band edge and deep trap emissions respectively. They observed that after annealing the band edge PL peak become more narrower, more symmetric and stronger than the as deposited one [16]. The same is observed in our case between the only Cu doped (sampleT4) and Cu,Mn doped (sampleT5) annealed at 350°C. The PL intensity at 428 nm is increased as compared to the unannealed samples and at 488 nm intensity is depressed. On the other hand, for sample T5 only emission has occurred at 442 nm and intensity of PL was found to increase which may be expected due to the presence of Mn ion. As reported by many researchers, that the presence of Mn^{2+} increase the photoluminescence intensity [36]. Furthermore, annealing remove the defects and stress present inside the crystal lattice and decrease the deep trap emission [16]. Inset of Fig 6.7 shows the PL spectra of undoped $Cd_{0.7}Zn_{0.3}S$ which was also given by the broad emission at 488 nm may be attributed to the emission from the sulphur vacancy state to the Zn defect states [37,38]. In the case of codoped sample $Cd_{0.7}Zn_{0.3}S$:Cu(0.01M),Mn(0.01M) at 350°C, the PL emission peak is found smooth and symmetrical with enhanced intensity as compared to the Cu doped $Cd_{0.7}Zn_{0.3}S$:Cu(0.01M) at 350°C and undoped sample $Cd_{0.7}Zn_{0.3}S$. Hence, less defects and strain may be believed as a consequence of codoping effects with Cu,Mn and annealing at 350°C of $Cd_{0.7}Zn_{0.3}S$ sample.

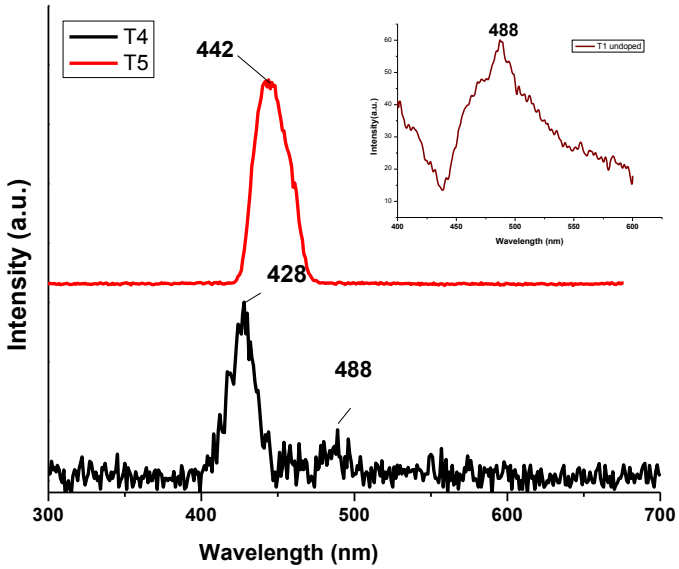

Fig. 6.7: The PL spectra of $Cd_{0.7}Zn_{0.3}S$:Cu and $Cd_{0.7}Zn_{0.3}S$:Cu,Mn annealed at 350°C (inset shows the emission spectra of undoped $Cd_{0.7}Zn_{0.3}S$).

Becker et al have observed blue emission band at 428 nm due to sulphur vacancies [39]. It is noted that PL peaks give emissions lower than the band gaps for sample T4,

T5 and undoped samples. This suggests that the transitions in our case occurred from the energy states lying inside the band gap as compared to band edge transitions. Furthermore, it is well reported that sulphur vacancies at surface gives rise to formation of zinc dangling bonds at shallow donor levels just below conduction band. The band gap energy was also calculated from the emission spectra using $E= hc/\lambda$, where λ is the emission wavelength and its value for sample T4 are obtained 2.89eV (428nm) and 2.54eV (488nm). However for the sample T5 its value is determined 2.80eV (442nm) that also confirms the transitions within the band gap. The PL peak broadening (FWHM~100 nm) for the undoped sample is typically observed for alloyed quantum dots [40]. Hence PL results also confirm that our almost prepared samples are quantum dot materials.

6.4 Conclusions

In conclusions, we have synthesized successfully undoped ternary alloy having composition $Cd_{0.7}Zn_{0.3}S$ and annealed this sample at 350°C. Further Cu doped and Cu,Mn co-doped samples were also annealed at 350°C. XRD of the prepared samples revealed the hexagonal structure. It has been concluded that in without dopant and as deposited, the lattice strain and dislocation density are found high ($\boldsymbol{\varepsilon}$ =0.0648, δ= 0.07980) as compared to the doped and annealed samples. The least strain has been obtained in the case of only Cu doped sample (T3); $Cd_{0.7}Zn_{0.3}S$ at 250°C as compared to the undoped T1, T2 (350°C) and co-doped T5(350°C) samples. Hence it may be concluded that the lattice strain and dislocation density decreases with temperature because with temperature surface defects are reduced. From the FTIR spectra, in lower energy region a small peak at wave number 657-676 cm^{-1} has been assigned to Cd-S/Zn-S stretching mode and also acetate group was confirmed in the range 1564-1533 cm^{-1}. TEM also show the spherical nanoparticles with size range larger than the XRD results. SAED pattern exhibits a set of rings rather than spots due to random orientation of crystallites, confirms the polycrystalline nature of the material. Further, The band gap calculated from the Tauc's relation by extrapolating the linear region of the plots to $(\alpha h\nu)^2 =0$ and their values for all sample determined in the range 3.75-5.17 eV. Band gap for undoped samples is obtained smaller than the annealed and doped samples. Furthermore, the PL spectra give emission in the blue green region at 428 nm and 488 nm. These two emissions peaks are due to sulphur vacancies and zinc defects presents in the system. In the case of codoped sample $Cd_{0.7}Zn_{0.3}S$:Cu(0.01M),Mn(0.01M) at

350°C, the PL emission peak is found smooth and symmetrical with enhanced intensity as compared to the Cu doped $Cd_{0.7}Zn_{0.3}S$:Cu(0.01M) at 350°C and undoped sample $Cd_{0.7}Zn_{0.3}S$. Hence, less defects and strain may be believed as a consequence of codoping effects with Cu,Mn and annealing at 350°C of $Cd_{0.7}Zn_{0.3}S$ sample.

References

[1] S.D. Chavhan, S. Senthilarasu, Soo-Hyoung Lee, Applied Surface Science **254** (2008) 4539–4545.

[2] M.C. Baykul and Orhan, Thin Solid Films **518** (2010) 1925.

[3] J. A. Rojas, A. I. Oliva, Materials and Manufacturing Processes, **30** (6) (2015), 785-792, DOI: 10.1080/10426914.2014. 994776.

[4] M. Jafary, R. Karimzadeh, M. Ghasemifard, Materials Science in Semiconductor Processing **32** (2015) 16–21 .

[5] R. Mariappan, M. Ragavendar, V. Ponnuswamy, Journal of Alloys and Compounds **509** (2011) 7337–7343.

[6] A. Bakhsh, I.H. Gul, A. Maqsood, C.H. Chan, S.H. Wu, Y.C. Chang, Chalcogenide Letters **13** (10) (2016) 443 – 450.

[7] G. Murali, D. Amaranatha Reddy, B. Poornaprakash, R. P. Vijayalakshmi, N. Madhusudhana Rao, Optoelectronics and Advanced Materials - Rapid Communications **5** (9) (2011) 928 – 931.

[8] S. Lee, D. Song, D. Kim, J. Lee, S. Kim, I.Y. Park, Y.D. Choi, Mater. Lett. **58** (2003) 357.

[9] T. Kuzuya, Y.Tai, S. Yamamuro, K.Sumiyana, Sci. Technol. Adv. Mater. **6** (2005) 84.

[10] P.B. Bagdare, S.B. Patil, A.K. Singh, J. Alloys Compd. **506** (2010) 120.

[11] H.C. Warad, S.C. Ghosh, B. Hemtanon, C. Thanachayanont, J. Dutta, Sci Technol Adv Mater. **6** (2005) 296.

[12] N. Manjula, M. Pugalenthi, V.S. Nagarethinam, K. Usharani, A.R. Balu, Materials Science-Poland **33** (4) (2015) 774-781.

[13] R.B. Kale, C.D. Lokhande, Semicond. Sci. Tech. **20** (2005) 1.

[14] A.R. West, Basic Solid State Chemistry, John Wiley & Sons Ltd, (1996).

[15] A. Vanaja, K. Srinivisa Rao, Advances in Nanoparticles **5** (2016) 83-89.

[16] C. Jin, W. Zhong, X.Zhang Y.Deng, C.Au, Y. Du, Crystal Growth and Design **9** (11) (2009) 4602-4606.

[17] M.F. Kotkata, A.E. Masoud, M.B. Mohamed, E.A. Mahmoud, Physica E **41** (2009) 1457.

[18] S. Kumar, J.K. Sharma, Materials Science-Poland **34** (2016) 368.

[19] X. Zou, E. Ying, and S. Dong, Nanotechnology **17** (2006) 4758.

[20] K. Manzoor, S. R. Vadera, N. Kumar, and T. R. N. Kutty, Solid State Commun. **129** (2004) 469.

[21] M Sharma , S. Kumar O. P. Pandey, J Nanopart Res **12** (2010) 2655-2666 .

[22] M. Sharma, T. Jain, S. Singh, and O. P. Pandey, AIP Advances **2** (2012) 012183.

[23] B. Akbari, M.P. Tavandashti, M .Zandrahimi, Iranian J. Mater. Sci. and Eng **8** (2011) 48-56.

[24] F. Antolini, E. Burresi, L. Stroea, V. Morandi, L. Ortolani, G. Accorsi, and M. Blosi, Journal of Nanomaterials (2012) Article ID 815696, 11 pages.

[25] G. Tai, J. Zhou, W. Guo, Nanotechnology, **21** (2010) 175601.

[26] O.O. Akinwunmi, G.O. Egharevba, E.O.B. Ajayi, Journal of Modern Physics **5** (2014) 257.

[27] T.P. Sharma, D. Patidar, N.S. Sexena and K. Sharma, Indian J. of Pure and Appl. Phys. **44** (2006) 125-128.

[28] J. Tauc, Amorphous and Liquid Semiconductor, J Tauc Edi, New York, Plenum, (1974).

[29] L. M. Kukreja, S. Barik, and P. Mishra, J. Cryst. Growth **268** (2004) 531.

[30] R. Shrivastava, S. C. Shrivastava Bull. Mater. Sci. **38** (5) (2015) 1277-1284.

[31] A. Jagannatha Reddy, M.K. Kokila, H. Nagabhushana, R.P.S. Chakradhar, C. Shivakumara, JL Rao, B.M. Nagabhushana, Journal of Alloys and Compounds **509** (2011) 5349-5355.

[32] K. Manzoor, S.R. Vadera, N. Kumar, T.R.N. Kutty Mater, Chem Phys. **82** (2003) 718.

[33] A.M. Salem, Applied Physics A **74** (2002) 205.

[34] M. Sharma, S. Singh, O. P. Pandey, J. Appl. Phys. **107** (2010) 104319.

[35] K. Jayanthi, S. Chawla, H. Chander, and D. Haranath, Cryst. Res. Technol.**42** (2007) 976

[36] T.Y. Lui, J.A. Zapien, H. Tang, D.D.D. Ma, Y.K. Liu, C.S. Lee, S.T. Lee, S.L. Shi and S.J. Xu, Nanotechnology **17** (2006) 5935-5940.

[37] W. Chen, R. Sammynaiken, Y. Huang, J.O. Malm, R. Wallenberg, J.O. Bovin, V. Zwiller, and A. N. Kotov, J. Appl. Phys. **89** (2001) 1120.

[38] T. Stoferle, S. Ullrich, R.F. Mahrt, Nano Lett. **9** (2009) 453.

[39] W.G. Becker, A.J. Bard, J. Phys. Chem. **87** (1983) 4888.

[40] M. Michalska, A. Aboulaich, G. Medjahdi, R. Mahiou, S. Jurga, R. Schneider, J. Alloy. Compd. **645** (2015) 184.